Heliyon 10 (2024) e26693

Contents lists available at ScienceDirect

Heliyon

journal homepage: www.cell.com/heliyon

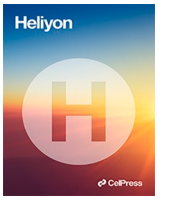

Research article

Enhanced dielectric properties of PVDF polymer nanocomposites: A study on gold−decorated, surface−modified multiwalled carbon nanotubes

Kaniknun Sreejivungsa , Prasit Thongbai *

Giant Dielectric and Computational Design Research Group (GD−CDR), Department of Physics, Institute of Nanomaterials Research and Innovation for Energy (IN−RIE), Khon Kaen University, Khon Kaen, 40002, Thailand

A R T I C L E I N F O

Keywords:
Multiwall carbon nanotubes
*n*Au−fMWCNTs
Turkevich method
Zeta potential
PVDF

A B S T R A C T

The integration of surface-modified multiwalled carbon nanotubes (fMWCNTs) into polymer nanocomposites has been extensively studied for their potential to enhance dielectric properties. This study, however, pioneers the use of a novel hybrid filler comprising fMWCNTs coated with metal nanoparticles, specifically aimed at augmenting the dielectric performance of polymers. In our research, poly(vinylidene fluoride) (PVDF) nanocomposite films were synthesized using fMWCNTs with a diameter of ~6–9 nm and a length of 5 μm, adorned with gold nanoparticles (*n*Au) of ~5.4 ± 0.9 nm *via* an adapted *Turkevich* method. Comprehensive analyses were conducted on *n*Au−fMWCNTs hybrid powder and their nanocomposites in PVDF with varying filler concentrations, confirming the formation of *n*Au−fMWCNTs with a weight ratio of 1.1 : 98.9. Three−phase percolative nanocomposites were produced by dispersing the hybrid filler in *N*, *N*−dimethylformamide, facilitated by interactions between the negative charge of *n*Au−fMWCNTs (zeta potential of ~ −40.43 ± 0.46 mV) and polar phases of PVDF. This was verified through zeta potential and Fourier−transform infrared spectroscopy analyses. The dielectric permittivity (ε') of the nanocomposites significantly increased from 17.8 to 524.8 (at 1 kHz) with filler loadings from 0.005 to 0.01 vol%, while the dielectric loss tangent (tanδ) showed a minor increase from 0.05 to 1.18. These enhancements are attributed to the elevated permittivity of *n*Au−fMWCNTs hybrid powder, PVDF's transition to the β−phase, and interfacial polarization effects. The restrained growth of *n*Au on fMWCNTs and the inhibition of conductive pathways in the polymer matrix contributed to the low tanδ values.

1. Introduction

Polymer nanocomposites have garnered significant attention as electronic materials due to their lightweight, exceptional electrical breakdown strength, and superior flexibility [1–4]. While ceramic materials typically exhibit superior dielectric properties [5,6], polymers tend to have dielectric constants (ε') lower than 10 [2,3]. Consequently, there was a focus on enhancing the properties of polymer materials to increase their ε' value, without compromising flexibility [7]. This enhancement is achieved by blending polymers with fillers, resulting in modified polymer composites suitable for electronic devices, charge storage capacitors, and transducers [1].

Poly(vinylidene fluoride) (PVDF) is a semicrystalline polymer renowned for its excellent chemical resistance, thermal stability, and

* Corresponding author.
E-mail address: pthongbai@kku.ac.th (P. Thongbai).

https://doi.org/10.1016/j.heliyon.2024.e26693
Received 6 December 2023; Received in revised form 21 January 2024; Accepted 18 February 2024
Available online 19 February 2024

a straightforward production process that requires lower temperatures compared to ceramic preparations. While PVDF possesses a ε' of around 10 and is extensively researched compared to other polymers [8,9], its ε' is insufficient for practical applications in electronic devices like capacitors. To enhance the ε' of PVDF, filler materials are often employed. A common approach to bolster the ε' of polymers involves combining them with high ε' ceramic materials such as $BaTiO_3$ [10], $BFeO_3$ (B═Bi and La) [11,12], $CaCu_3Ti_4O_{12}$ [13], and $ACu_3Ti_4O_{12}$ (A = Ca, $Na_{0.5}Bi_{0.5}$, $Na_{0.5}Y_{0.5}$, and $Na_{0.33}Ca_{0.33}Bi_{0.33}$) [14–17]. Regrettably, achieving high ε' values in polymer composite systems often requires a high ceramic material content of about 50 vol% [18,19]. This high content compromises the mechanical integrity of the polymer, resulting in reduced flexibility [20], compromised processability, and an elevated defect density.

To address the issues associated with traditional fillers, conductive fillers like metal particles, carbon nanotubes [1], carbon black, and carbon fiber [21] have been extensively incorporated into polymer composites to elevate ε' values [22,23]. Through this method, a high ε' can be attained. Furthermore, the dielectric properties of composites quickly change as the content of conductive fillers increases, often achieving a threshold well below 50 vol%. Multiwall carbon nanotubes (MWCNTs) in particular have been integrated into polymer matrices like percolative composites [21] due to their lightweight properties, substantial aspect ratios, and vast internal surface areas [24]. This results in lower percolation thresholds in composites, enhancing the ε' value. Notably, MWCNTs not only elevate the ε' but also allow the polymer to retain its flexibility. When formulating two-phase MWCNTs/PVDF composites with a random system, the percolation threshold for MWCNTs aligns with a volume fraction (f) of 0.0161 [25]. In this case, the ε' value of the MWCNTs/PVDF composite was ~50 and the loss tangent (tanδ) was ~0.3 at 1 kHz. Notably, on increasing the f_{MWCNTs} fron 0.016 to 0.02, although the ε' value rapidly increased to ~300. Concurrently, there was a rapid increase in conductivity by two orders of magnitude, leading to a substantial rise in the tanδ value. Similarly, other previous studies have also demonstrated that while MWCNTs in polymer composites can raise the ε' value, it also leads to a significant increase in the tanδ of >10 [26–28]. This is because MWCNTs, with their carbon chain structure, can create conductive pathways in the polymer matrix, thereby enhancing conductivity and tanδ, which might not be ideal for all applications. Additionally, a significant barrier with MWCNTs is their poor solubility and processability due to the van der Waals reactions [29,30], and their high surface area aspect ratio often results in self−aggregation [31]. To overcome the self−aggregation of MWCNTs, surfactants [32] were utilized to enhance their dispersibility. Additionally, chemical modifications, particularly the introduction of carboxyl groups on the surfaces of MWCNTs [33], have been shown to improve their distribution within slurries. Such modifications often involve acidic treatments, as extensively documented in the literature [30, 33–35]. Furthermore, functionalization stands out as a pivotal strategy to inhibit the self−aggregation of carbon nanotubes. This can be achieved through both noncovalent and covalent means, each significantly enhancing the solubility and dispersal of carbon nanotubes [36]. Sheih et al. [37] observed that the dispersion of carbon nanotubes in solvents like water is markedly improved when they are covalently functionalized, attributing this to the ionization of carboxylic (COOH) groups on the treated nanotubes. In cases where strong acid treatments are employed, such as with nitric [38], sulfuric acid, and nitric acid [30], the attachment of carboxylic groups imparts hydrophilic characteristics to the nanotubes, leading to a markedly more effective dispersion.

To enhance the ε' while maintaining a low tanδ in polymer nanocomposites, one strategy is to incorporate a hybrid filler. This hybrid filler combines a primary component of carbon nanotubes with a high ε' value, with metal nanoparticles serving as a secondary filler. The synergy between MWCNTs and nanoparticles has garnered considerable interest due to the novel properties that these hybrid nanostructures exhibit, representing the best of both constituent materials. For the integration of MWCNTs with metal nanoparticles, noble metals such as Pt, Pd, Ag, and Au are particularly promising for enhancing the performance of nanocomposites [39]. These metal nanoparticles are not only easy to synthesize but can also be functionalized with various molecules or groups. Notable developments include the formation of gold−decorated multi−walled carbon nanotubes (Au−MWCNTs) [40–42], silver nanoparticle decoration on multiwalled carbon nanotubes (Ag/CNT) [38], and MWCNTs adorned with Ag nanoparticles (MWCNTs−Ag) [30]. Such hybrid fillers are beneficial as they disrupt the formation of conductive pathways, which in turn hinders the development of a conducting network within composites like MWCNTs/PVDF and Ag nanoparticles (Ag−NPs), potentially inducing the Coulomb blockade effect [1].

Recent studies have indicated that the dielectric properties of PVDF polymer nanocomposites can be substantially improved by incorporating such hybrid particles, as seen in Au−MWCNT [43], and Ag–Cu/MWCNTs/reduced graphene oxide (rGO) nanocomposites [44]. However, the dielectric property variation with temperature in Au−MWCNT/PVDF nanocomposites remains unreported [43], which is a crucial aspect for their practical application. For dielectric polymer composites, Au nanoparticles are suitably selected to decorate MWCNTs for their suitable electrical properties and high thermal stability (318 W/mK). Compared to SiO_2, which has a thermal stability of 1.3 W/mK, Au serves as a more effective filler for the composites in electronics due to its crucial role in effective heat management in electronic devices. Au nanoparticles with sizes of 10–50 nm exhibit decreased conductivity ($1.5–2.2 \times 10^{-2}$ S/m) [45] due to the Coulomb blocking effect, in contrast to SiO_2 at approximately 10^{-10} S/m. This difference in conductivity between PVDF and Au nanoparticles enables interfacial polarization, unachievable with SiO_2.

Using the concept of modified MWCNT surface, functionalized MWCNTs (**f**MWCNTs) treated with 3,4,5-trifluorobromobenzene were employed as a filler to augment the dielectric properties of PVDF matrix composites. Dang et al. [46] demonstrated that the ε' value of the **f**MWCNTs/PVDF composite, with $f_{fMWCNTs} = 0.08$, was ~550 at 1 kHz, while the tanδ was ~2.2. Additionally, it has been reported that PVDF composites filled with surface-modified MWNTs, featuring a core/shell structure, exhibited an increased ε' of ~600 at 100 Hz [26]. Despite the surface modification of MWCNTs, maintaining control over the conductive pathway remains challenging, often resulting in high conductivity and tanδ.

According to the Coulomb blocking effect observed in Au nanoparticles, it is hypothesized that these nanoparticles could impede the formation of conductive pathways, thereby restraining increases in conductivity and tanδ. Integrating Au with MWCNTs is expected to significantly enhance the dielectric and thermal properties of the nanocomposite, optimizing the performance of PVDF composites. The stability and compatibility of Au with the PVDF matrix, coupled with easier surface decoration on modified MWCNTs,

ensure consistent nanocomposite properties. The study aims to reduce dielectric loss and minimize loss tangent, considering the moderate conductivity of Au.

In this study, we introduce a novel approach whereby gold nanoparticles (*n*Au) are systematically assembled on the surface of functionalized multi-walled carbon nanotubes (**f**MWCNTs) using a modified *Turkevich* method. The resulting nAu−decorated fMWCNTs (abbreviated as *n*Au−**f**MWCNTs) hybrid powder was synthesized by first functionalizing MWCNTs with carboxylate groups (COO^-) to create **f**MWCNTs, which then attract Au^{3+} ions through electrostatic interactions. Although the functionalization of MWCNTs using nitric acid is less common compared to the dual treatment with sulfuric and nitric acids [33,43,44,47], research by Datsyuk et al. [35] has demonstrated that nitric acid treatment alone can result in a higher relative concentration of carboxylic groups, as determined by titration, in comparison to other acids. This finding underscores the potential of nitric acid modification to significantly enhance the functionality of MWCNTs for the synthesis of complex nanocomposites. *n*Au nanoparticles, averaging approximately 5.4 ± 0.9 nm in size, were intermittently affixed to the surface of **f**MWCNTs. These *n*Au−**f**MWCNT hybrid powders were subsequently incorporated as fillers into a PVDF polymer matrix. The resulting composites underwent extensive characterization using various analytical techniques. Additionally, their dielectric properties were meticulously examined with respect to both frequency and temperature.

2. Experimental details

2.1. Materials

Gold (III) chloride trihydrate (purity: ≥99.9%; $HAuCl_4{\cdot}3H_2O$) was bought from Sigma Aldrich (Sigma–Aldrich Co., (St. Louis, MO, USA)). Multiwall carbon nanotubes (MWCNTs) (6 − 9 nm in diameter, 5 μm in length) (purity: ≥95%) were bought from Sigma Aldrich (Sigma–Aldrich Co., (St. Louis, MO, USA). Poly (vinylidene fluoride) (PVDF) average MW∼ 534,000 was bought from Sigma Aldrich (Sigma–Aldrich Co., (St. Louis, MO, France)). Sodium citrate tribasic sesquihydrate (purity: ≥99%: $C_6H_5Na_3O_7 \cdot 2H_2O$) was bought from Sigma Aldrich (Sigma–Aldrich Co, Hamburg, Germany). *N, N*−dimethylformamide (purity: >99%, $HCON(CH_3)_2$; DMF), and Hydrochloric acid 37% (HCl) were bought from RCI Labscan (RCI LABSCAN LTD., (24 Rama 1 Rd. Rong Mueang, Pathumwan, Bangkok, Thailand)). Nitric acid 65% (HNO_3) and Sodium hydroxide (purity: ≥99; NaOH) were bought from Merck (Merck Chemicals, Darmstadt, Germany).

2.2. Functionalized of MWCNTs

To produce oxidized MWCNTs or MWCNTs−COOH, 3 g of pristine MWCNTs were suspended in 250 mL of nitric acid and sonicated for 2 h then stirred the suspension for 48 h at ∼25 °C. The resulting suspension was centrifuged with deionized water until the neutral pH was obtained. At last, the MWCNTs−COOH was obtained and dried at 80 °C overnight [35,38].

MWCNTs−COOH were suspended in 250 mL of 0.04 N of NaOH and sonicated for 2 h then the suspension was stirred for 48 h at ∼25 °C. The resulting suspension was centrifuged with deionized water until the neutral pH was obtained. At last, the carboxyl group into carboxylate (MWCNTs−COO^- or **f**MWCNTs) was obtained. After that the product was dried at 80 °C overnight [35,38].

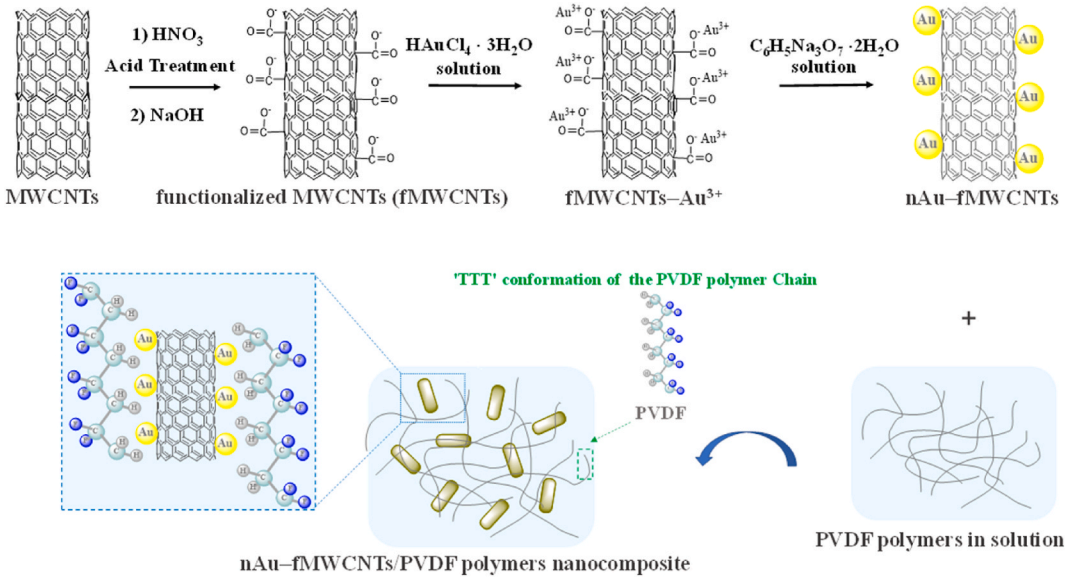

Fig. 1. Schematic diagram of the formation of *n*Au−**f**MWCNTs polymer nanocomposites.

2.3. Preparation of nAu–fMWCNTs hybrid powder

The *n*Au–**f**MWCNTs hybrid powder was prepared by the modified *Turkevich* method [48]. To produce *n*Au–**f**MWCNTs, first, 0.5g **f**MWCNTs were suspended in 25 mL deionized water, and the suspension was stirred for 30 min at ~25 °C and sonicated for 30 min with dispersing **f**MWCNTs well. Second, 500 μL of $HAuCl_4{\cdot}3H_2O$ (1 mM) were added to the solution and sonicated for 1 h then the suspension was stirred and heated to boiling while stirring. Third, 4 mL of $C_6H_5Na_3O_7{\cdot}2H_2O$ (38.8 mM) was added to the suspended solution. The mixture was further stirred until it became red. The solution was cool at ~25 °C. The resulting suspension was centrifuged and washed several times (10 × 30 mL) with deionized water. At last, the obtained *n*Au–**f**MWCNTs hybrid powder was dried at 80 °C overnight [49]. Moreover, the prepared *n*Au–**f**MWCNTs hybrid powder was examined for a surface charge of particles by the Zetasizer technique. Fig. 1 shows the schematic illustration synthesis of *n*Au–**f**MWCNTs. UV–vis spectroscopy and TEM techniques confirm that all *n*Au nanoparticles had been decorated on the surface of **f**MWCNTs.

2.4. Preparation of nAu–fMWCNTs/PVDF polymer nanocomposites films

The volume fractions of the PVDF matrix and fillers were calculated by the following equation:

$$\%(n\text{Au-}\mathbf{f}\text{MWCNTs})\text{ by weight} = \frac{V_{\text{nAu-fMWCNTs}}\,\rho_{\text{nAu-fMWCNTs}}}{V_{\text{nAu-fMWCNTs}}\,\rho_{\text{nAu-fMWCNTs}} + (1-V_{\text{PVDF}})\,\rho_{\text{PVDF}}} \times 100, \quad (1)$$

where $V_{nAu-fMWCNTs}$ is the percentage of *n*Au–**f**MWCNTs by volume, $\rho_{nAu-fMWCNTS}$ is the theoretical density of *n*Au–**f**MWCNTs, ρ_{PVDF} is the density of the PVDF polymer (1.74 g/cm^3). The $\rho_{nAu-fMWCNTs}$ were calculated from the following Equation:

$$\rho_{nAu-fMWCNTs} = \rho_{fMWCNTs} V_{fMWCNTs} + \rho_{nAu} V_{nAu}\ , \quad (2)$$

where $\rho_{fMWCNTs}$ and ρ_{nAu} are the **f**MWCNTs (2.1 g/cm^3) and nAu (19.3 g/cm^3), respectively. $V_{fMWCNTs}$ and V_{nAu} are the volume fractions of the **f**MWCNTs and nAu, respectively. We showed that the percentage ratio of *n*Au: **f**MWCNTs was obtained to be 1.1: 98.9 wt%. By using Equations (5.1) and (5.2), the $\rho_{nAu-fMWCNTs}$ were calculated and found to be 2.12 g/cm^3. Thus, the nanocomposites with different volume fractions of *n*Au–**f**MWCNTs hybrid powder can be designed in the experimental using Equation (5.1). The

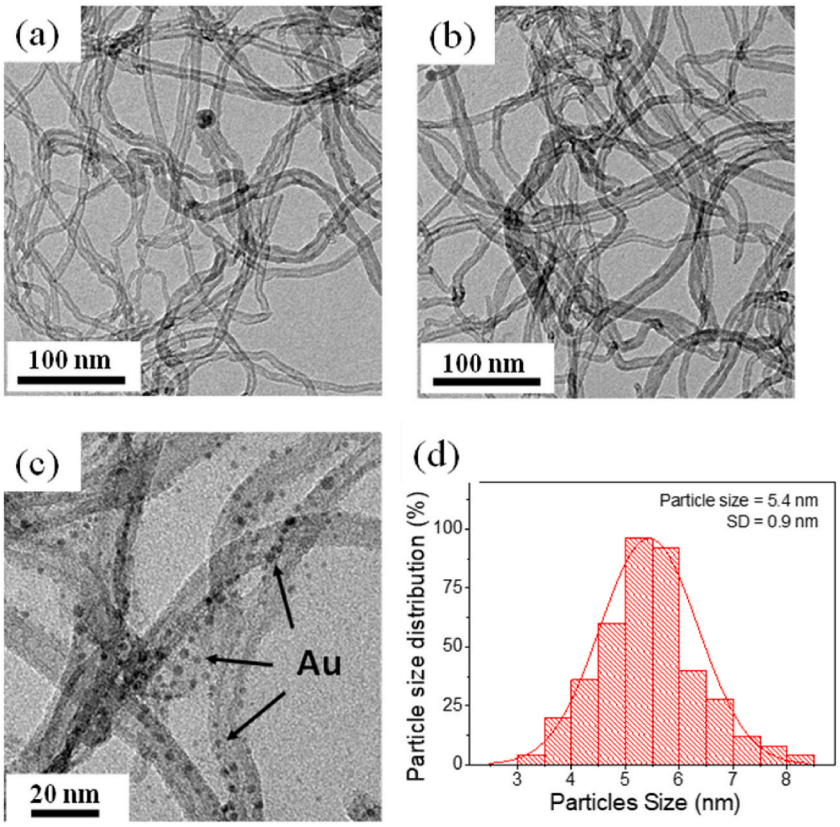

Fig. 2. TEM images of (a) MWCNTs, (b) **f**MWCNTs, and (c) *n*Au–**f**MWCNTs particles. (d) Size distribution of *n*Au nanoparticles deposited on **f**MWCNTs.

*n*Au−**f**MWCNTs/PVDF polymer nanocomposites were prepared by suspending an appropriate amount of PVDF powder in DMF with stirring for 30 min. Similarly, the nAu−fMWCNTs powder was also dissolved in DMF with ultrasonic treatment for 1 h. The mixture solution was stirred further using ultrasonic bath for 1 h and further stirring for 6 h with a dispersion of *n*Au−**f**MWCNTs nanoparticles. The mixture was then dried in an oven at 70 °C [50]. Polymer nanocomposites films were obtained by hot−pressing at 200 °C for 30 min with compression of 10 MPa to eliminate defects (i.e., Porous) to obtain a *n*Au−**f**MWCNTs/PVDF polymer nanocomposites films.

2.5. Characterization techniques and dielectric measurements

The morphologies of MWCNTs, **f**MWCNTs, and *n*Au−**f**MWCNTs hybrid powders were characterized using a transmission electron microscope (TEM, TECNCI G^2 20) operating at an accelerating voltage of 200 kV. For sample preparation, these powders were suspended in ethanol and sonicated for 2 h to ensure a homogeneous dispersion. The resulting suspension was then deposited onto a copper grid for TEM analysis. The amount of *n*Au nanoparticles attached on surface carbon nanotube nanoparticles was determined using UV–vis absorption spectroscopy (Shimadzu, UV−1800). Stability and surface charge of MWCNTs, **f**MWCNTs, and *n*Au−**f**MWCNTs hybrid powder were studied using Zeta potential estimation from Zetasizer (ZS−90 Malvern Instruments). The phase ingredient of MWCNTs, **f**MWCNTs, *n*Au−**f**MWCNTs hybrid powder, and *n*Au−**f**MWCNTs/PVDF nanocomposites were examined using an X−ray Diffractometer (XRD; PANalytical, EMPYREAN). The phase of PVDF matrix and functional groups on the surfaces of **f**MWCNTs were verified by Fourier transform infrared spectroscopy (FTIR, TENSOR27) in the wavenumber range of 600–4000 cm^{-1}. The morphology of *n*Au−**f**MWCNTs/PVDF nanocomposites was studied by focus ion beam–field emission scanning electron microscopy (FIB−FESEM, FEI Helios NanoLab G3 CX). Both surfaces of disk sample were painted with silver glue and dried at 100 °C for 30 min for dielectric measurements. Dielectric properties were studied using Impedance Analyzer (KEYSIGHT, E4990A, Santa Rosa, CA, USA) in the frequency range of 100 Hz to 10 MHz at ~25 °C. The oscillation voltage was 0.5 V.

3. Result and discussion

TEM has been utilized to characterize the morphologies of MWCNTs, **f**MWCNTs, and *n*Au−**f**MWCNTs hybrid fillers. Fig. 2(a) presents the pristine MWCNTs, which display entangled, fibrous structures with a notable aspect ratio, free from any additional particles or discernible surface modifications, signifying their unmodified state. These pristine MWCNTs have a diameter ranging from 6 to 9 nm, which emphasizes the retention of their intrinsic morphology following functionalization. Fig. 2(b) illustrates the morphology of **f**MWCNTs. In comparison to the pristine MWCNTs, the **f**MWCNTs may exhibit a slightly altered contrast owing to the presence of functional groups or other molecular entities on their surface, though such details may not be distinguishable at the given scale or resolution. This suggests that acid treatment predominantly affects the surface chemistry and charge of the MWCNTs without altering their overall structure, as evidenced by the consistent diameter range of 6–9 nm for both variants. Fig. 2(c) shows MWCNTs that have been functionalized and subsequently embellished with *n*Au particles (*n*Au−**f**MWCNTs), with the dark spots marked by arrows corresponding to the *n*Au particles, averaging approximately 5.4 ± 0.9 nm in size, as determined in Fig. 2(d). The *n*Au particles were discontinuously attached to the surface of the **f**MWCNTs. The size of these particles is subject to a variety of factors, including the type of surfactant used, preparation temperature, concentration of $HAuCl_4{\cdot}3H_2O$ [51], type of reducing agent, presence of capping ligand [52], concentration of reducing agents [53], and the methodologies and pH levels applied during the preparation process [54,55]. The attachment of Au nanoparticles to the surface of fMWCNTs, which is noteworthy, could significantly influence the functional properties of the resultant hybrid materials.

Zeta potential represents the potential difference between the charged surfaces of carbon nanotubes and the surrounding liquid. This value is associated with the stability of carbon nanotubes in a dispersion medium, indicating the repulsive forces present in the suspension environment. Factors such as size, shape, and surface charge significantly affect the dispersion of colloidal nanoparticles. The stability of these nanoparticles in solution is generally indicated by a zeta potential value greater than ±30 mV [56], suggesting stable dispersion without particle aggregation. Conversely, colloids with low zeta potential are prone to coagulation. Table 1 presents the zeta potential values for pristine MWCNTs, functionalized MWCNTs, acid−treated MWCNTs, and *n*Au−**f**MWCNTs in an aqueous medium. The zeta potential of **f**MWCNTs is influenced by the carboxyl groups (COOH) on the MWCNTs surface. In the case of *n*Au−**f**MWCNTs, a high negative zeta potential is observed, attributable to the combined effects of carboxyl groups on the carbon nanotubes and the negatively charged *n*Au.

Fig. 3(a)−(d) illustrate the dispersibility behavior of pristine MWCNTs, **f**MWCNTs, and *n*Au-**f**MWCNTs at a concentration of 0.05 mg/mL in water, observed after sonication for time periods of 1 h, 1 day, 14 days, and 28 days, respectively. It was found that MWCNTs, which possess a low concentration of COOH groups, exhibit poor dispersion and stability in water over time, ranging from 1 h to 28 days. This behavior is further analyzed and described in the context of zeta potential measurements and will be elaborated upon in the FTIR analysis section. Conversely, **f**MWCNTs and *n*Au-**f**MWCNTs, which contain a higher concentration of COOH groups due to

Table 1
Zeta potential of MWCNTs, **f**MWCNTs, and *n*Au−**f**MWCNTs.

Specimen	Average zeta potential (mV)	Solution
MWCNTs	−22.17 ± 0.76	DI water
fMWCNTs	−38.10 ± 0.66	DI water
*n*Au−**f**MWCNTs	−40.43 ± 0.46	DI water

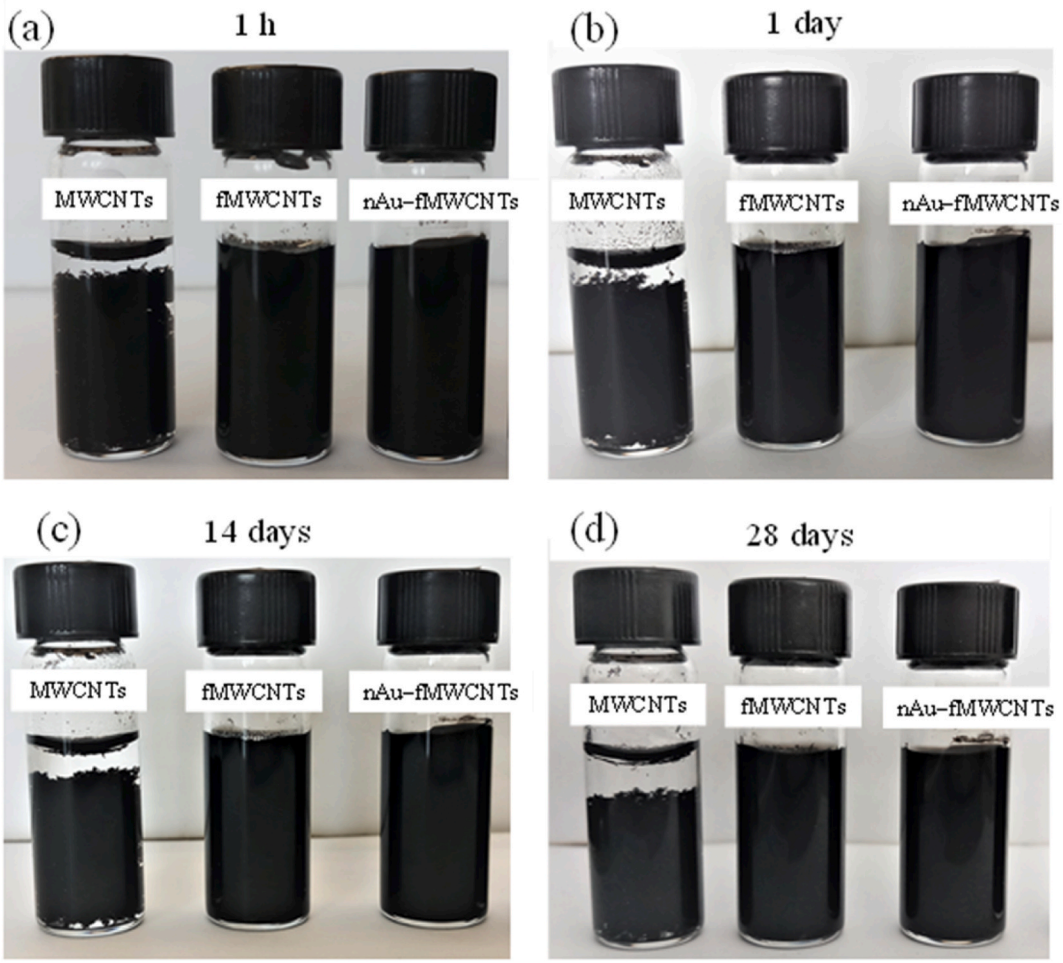

Fig. 3. Dispersibility behavior of the 0.05 mg/mL of nanofluid, (a) 1 h after sonication, (b) 1 day after sonication, (c) 14 days after sonication, and 28 days after sonication. (Pristine MWCNTs (left), acid−treated MWCNTs (middle) and *n*Au−fMWCNTs (right)).

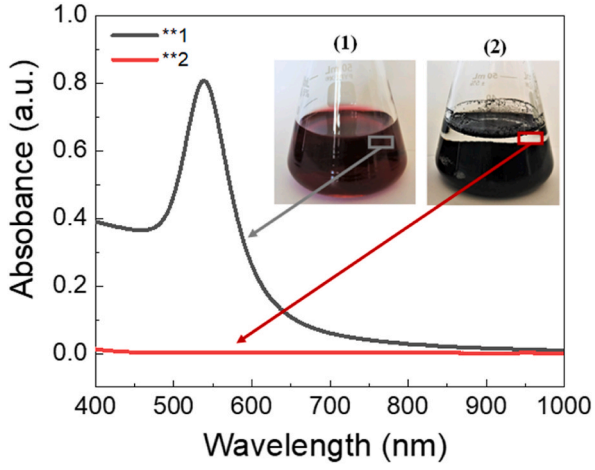

Fig. 4. UV–vis spectra of AuNPs and *n*Au−fMWCNTs hybrid powder synthesized by a *Turkevich* method.

the presence of COO^- and H^+ ions, demonstrate significantly different repulsion forces and enhanced stability in water over the same periods. This increased stability is attributed to their higher zeta potential values.

Fig. 4 displays the successful attachment of *n*Au particles on the surface of **f**MWCNTs, as verified by UV–vis spectroscopy to confirm the presence of *n*Au. The maximum absorption peak is observed at a wavelength of approximately 520 nm [57], aligning with the absorption peak reported in the literature [58,59]. This is illustrated by the red−colored solution in inset (1) of Fig. 4. Following centrifugation, which sediments the *n*Au−**f**MWCNTs powder, the resultant clear solution is again analyzed using UV–vis spectroscopy. Inset (2) in Fig. 4 demonstrates that almost all *n*Au particles are attached to the surface of **f**MWCNTs, indicated by the absence of *n*Au absorption. This finding is in agreement with observations from the TEM image shown in Fig. 2(c). Therefore, the ratio of *n*Au to **f**MWCNTs in the *n*Au−**f**MWCNTs hybrid powder is deduced to be 1.1 : 98.9 wt%.

Fig. 5 presents the XRD patterns within the 2θ range of 10°–80° for three types of powders: MWCNTs, **f**MWCNTs, and *n*Au−**f**MWCNTs. For MWCNTs, distinct diffraction peaks are observed at 2θ values of 26.5° and 42.7°. These peaks correspond to the (002) and (100) crystallographic planes of graphite, as identified in the JCPDS file 01−0646 [60]. The XRD patterns of **f**MWCNTs are similar to those of MWCNTs, indicating no significant alteration in the crystalline structure upon functionalization. Additionally, the XRD spectrum of *n*Au-**f**MWCNTs shows characteristic peaks corresponding to the (111), (200), (220), and (311) planes of gold (Au), as referenced in the JCPDS file 00−001−1172. This confirms the successful incorporation of *n*Au in the *n*Au−**f**MWCNTs hybrid powder.

FTIR was utilized to identify the functional groups on the surfaces of MWCNTs, treated in various ways, within the range of 700–4000 cm^{-1}, as depicted in Fig. 6. The FTIR spectra of MWCNTs reveal a broad peak at 1640 cm^{-1}, which is indicative of the carbonyl group of the quinone type on the surface of MWCNTs. This could result from oxidation during fabrication. The stretching band at 1460 cm^{-1}, corresponding to the methylene (CH_2) group [38], is observed. Additionally, peaks at 2920 and 2850 cm^{-1} are also evident in the MWCNTs spectra [34,38]. In the case of **f**MWCNTs, the carboxylic stretching of C═O at 1720 cm^{-1} indicates the formation of carboxylic groups by oxidation of partial carbon atoms on the MWCNT surface due to nitric acid treatment. The C═C stretching peak observed at 1460 cm^{-1} is diminished due to this nitric acid exposure. Signals between 1050 and 1300 cm^{-1} may be associated with C–O stretching, originating from lactones, carboxylic acids, alcohols, and other functional groups [38].

The *n*Au–**f**MWCNTs hybrid powder was characterized through elemental mapping and EDS using FIB–FESEM, conducted without an Au sputter coating. Fig. 7(a) displays the FE–SEM images of the *n*Au–**f**MWCNTs hybrid powder. Fig. 7(b) and (c) present the mapping images, illustrating the homogenous dispersion of C and Au in the *n*Au–**f**MWCNTs hybrid powder.

The FE−SEM cross−sectional image of *n*Au−**f**MWCNTs/PVDF nanocomposite, with a $f_{nAu-fMWCTs} = 0.008$, is depicted in Fig. 8. The surface morphologies are characterized as dense and smooth, attributable to the homogeneous dispersion of fillers within the polymer matrix. Additionally, the **f**MWCNTs are randomly dispersed throughout the polymer matrix. The dielectric properties of the nanocomposites are influenced by the distribution of the fillers and the presence of defects, such as pores. The agglomeration of fillers tends to increase the tanδ value, leading to higher current leakage.

fMWCNTs/PVDF nanocomposites films with $f_{fMWCTs} = 0.005$, 0.01,0.015 and 0.02, as well as *n*Au−**f**MWCNTsPVDF nanocomposite films with $f_{nAu-fMWCTs} = 0.005$, 0.006, 0.007, 0.008, 0.009, 0.01, 0.015 and 0.02, demonstrate notable flexibility. This characteristic of the polymer nanocomposite films is clearly exhibited in Fig. 9.

The phase structures of pure PVDF polymer and *n*Au−**f**MWCNTs/PVDF nanocomposites with $f_{nAu-fMWCNTs} = 0.5$, 1.0, and 1.5 vol% were examined using XRD, as shown in Fig. 10. The *n*Au−**f**MWCNTs/PVDF nanocomposites retain the characteristic patterns of the base polymer. In the γ−phase of PVDF polymer films, diffraction peaks are observed at a 2θ angle of 18.5°, corresponding to the (020) plane. The polar β−phase is characterized by diffraction peaks at 20.8° and 36.6°, aligning with the (110) and (020) planes, respectively [2,3,61,62]. The XRD results lead to the conclusion that the structure of polymer remains unchanged by the chemical treatment.

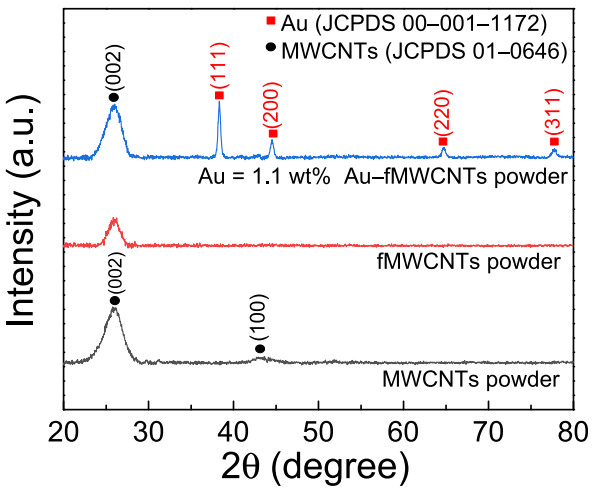

Fig. 5. XRD patterns of MWCNTs powder, **f**MWCNTs powder, and *n*Au−**f**MWCNTs hybrid powder.

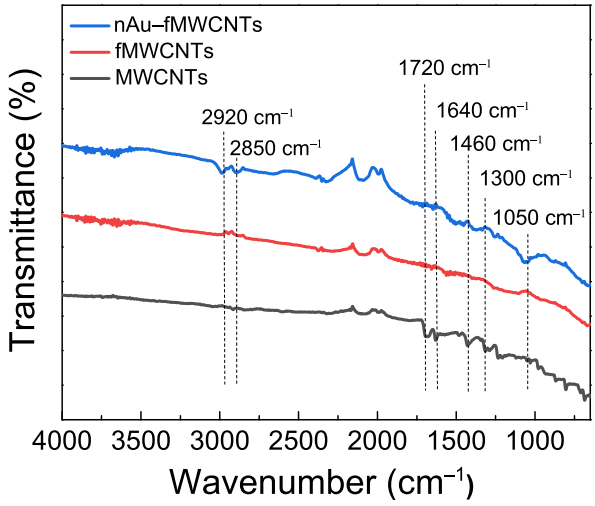

Fig. 6. FTIR spectra of pristine MWCNTs, acid−treated MWCNTs, and *n*Au−**f**MWCNTs.

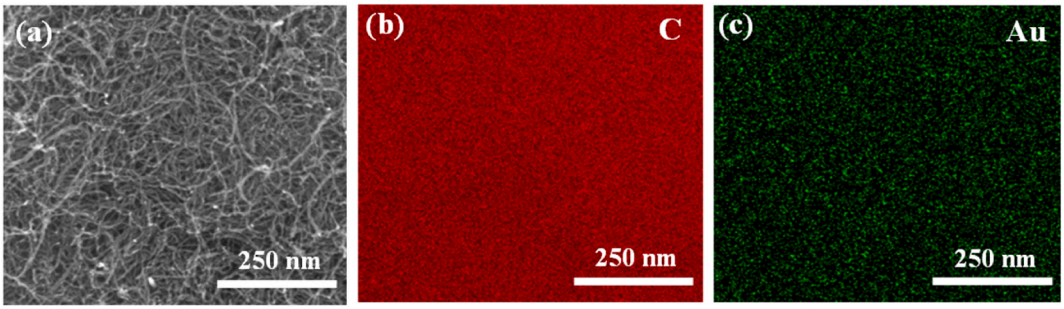

Fig. 7. (a) FE−SEM images of *n*Au−**f**MWCNTs hybrid powder. (b) and (c) FE−SEM mapping elements of C and Au, respectively.

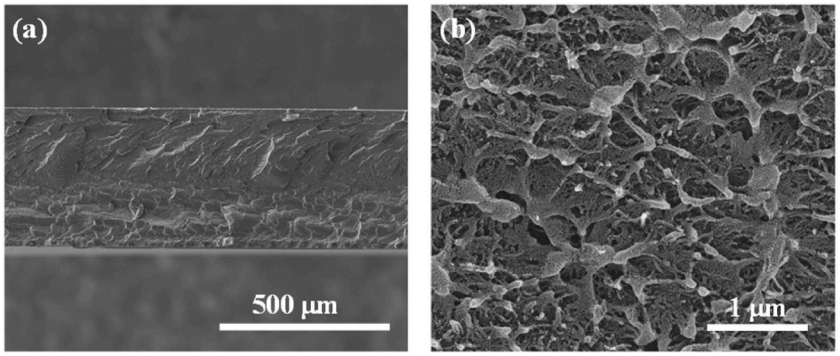

Fig. 8. FE−SEM images of fractured surface for *n*Au−**f**MWCNTs/PVDF nanocomposite with $f_{nAu-fMWCTs} = 0.008$ (a and b).

Fig. 11(a) illustrates the frequency dependence of the ε' for both PVDF and *n*Au−**f**MWCNTs/PVDF nanocomposites at varying levels of $f_{nAu-fMWCNTs}$, in comparison to MWCNTs/PVDF nanocomposites. As detailed in Table 2 and depicted in Fig. 11(a), it is observed that the ε' value of the *n*Au−**f**MWCNTs/PVDF nanocomposites exhibits an increase with the rising $f_{nAu-fMWCNTs}$ content. This suggests that the *n*Au−**f**MWCNTs hybrid fillers are capable of enhancing the dielectric response in the PVDF polymer. However, it is observed that the ε' values of the *n*Au−fMWCNTs/PVDF nanocomposites with filler volume fractions of 0.005 and 0.010 are lower than those of the MWCNTs/PVDF nanocomposites at the same volume fractions. Additionally, as detailed in Table 2 and shown in Fig. 11(b), the tanδ values of the *n*Au−**f**MWCNTs/PVDF nanocomposites are markedly lower than those of the MWCNTs/PVDF nanocomposites, exhibiting a difference of 2–3 orders of magnitude across all filler volume fractions. It is important to recognize that low−dimensional systems in nanomaterials, such as Au nanoparticles, exhibit electronic discontinuity and possess quantized values. The quantification

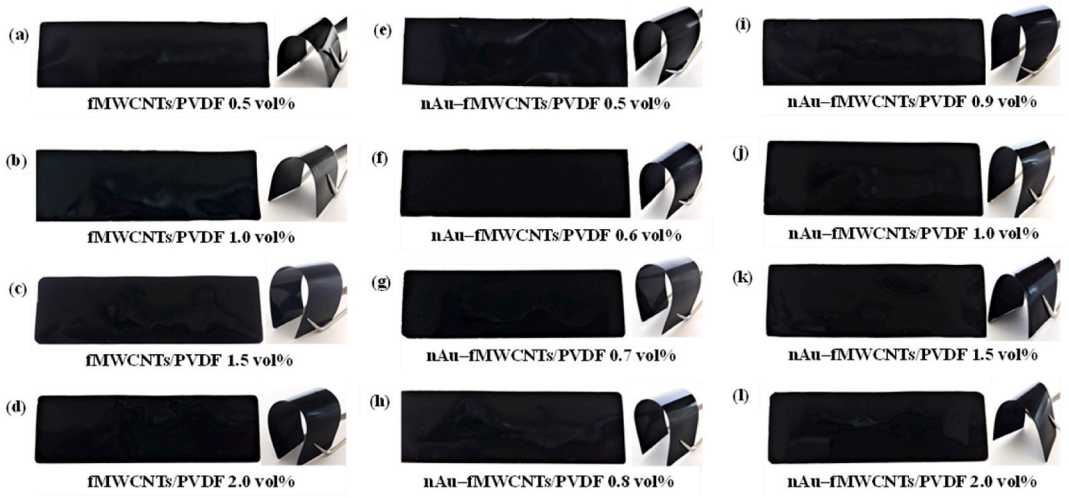

Fig. 9. Photo images of (a–d) **f**MWCNTs/PVDF and (e–l) *n*Au−**f**MWCNTs/PVDF nanocomposite films.

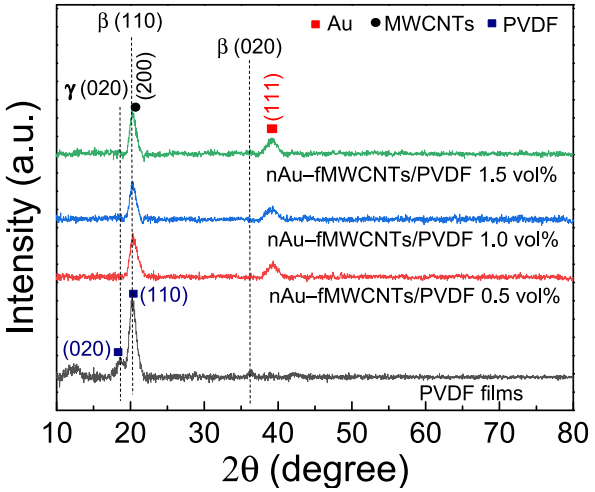

Fig. 10. XRD patterns of PVDF and *n*Au−**f**MWCNTs/PVDF nanocomposites with various contents of *n*Au−**f**MWCNTs.

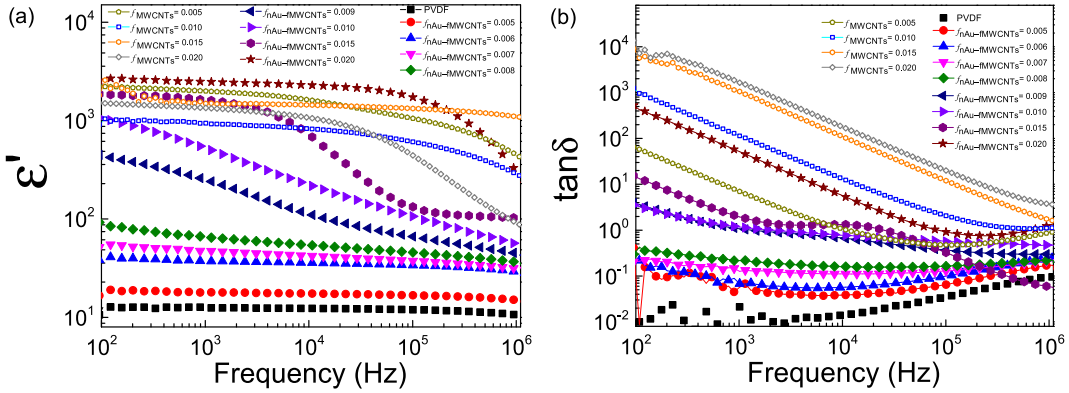

Fig. 11. Frequency dependence at ~25 °C of (a) ε' and (b) tanδ for *n*Au−**f**MWCNTs/PVDF nanocomposites with various contents of *n*Au−**f**MWCNTs hybrids fillers compared to MWCNTs/PVDF nanocomposites.

Table 2
β−phase fraction (F(β)), ε', tanδ, and σ_{ac} of MWCNTs/PVDF, **f**MWCNTs/PVDF and *n*Au−**f**MWCNTs/PVDF polymer nanocomposites films at 1 kHz and 25 °C.

Volume fraction	*F*(β) (%)	ε'	tanδ	σ_{ac} (S.cm^{-1})
PVDF	66	12.5	0.021	1.50×10^{-8}
MWCNTs				
0.005	62	1991.7	6.97	7.82×10^{-4}
0.010	60	940.4	113.91	6.03×10^{-3}
0.015	–	1487.2	1054.42	8.83×10^{-2}
0.020	52	1343.5	1636.15	1.24×10^{-1}
fMWCNTs				
0.005	62	902.4	0.834	4.23×10^{-5}
0.010	58	911.8	2.813	1.44×10^{-4}
0.015	52	1709.3	2.163	2.08×10^{-4}
0.020	52	2571.4	79.61	1.15×10^{-2}
*n*Au−*f*MWCNTs				
0.005	63	17.8	0.057	5.74×10^{-8}
0.006	–	37.6	0.068	1.43×10^{-7}
0.007	–	47.6	0.126	3.37×10^{-7}
0.008	–	65.3	0.216	7.95×10^{-7}
0.009	–	250.8	1.070	1.51×10^{-5}
0.010	57	524.8	1.175	3.47×10^{-5}
0.015	53	1621.8	1.950	1.78×10^{-4}
0.020	51	2477.4	51.345	7.16×10^{-3}

of electronic status in these materials leads to the emergence of novel characteristics and phenomena, including the effects of quantum confinement and Coulomb blockade, as detailed in Ref. [63]. Significant blocked charges occur at the interfaces between **f**MWCNTs−PVDF and *n*Au−PVDF, which can be attributed to interfacial polarization or the Maxwell−Wagner−Sillars (MWS) effect, particularly at the interfaces of PVDF−*n*Au and **f**MWCNTs−*n*Au [64]. The **f**MWCNTs, composed of long−chain carbon, can create random arrangements and conductivity paths. This leads to increased tanδ values due to the change in conductivity as the proportion of fillers increases. The MWS effect involves independent charges located on discrete surfaces between insulated phases, enhancing conductivity. Under an applied electric field, dipoles can form, significantly improving the dielectric response of three−phase nanocomposites. In a random two−phase system, the percolation threshold for conducting spherical particle fillers is around 16 vol% [24,25]. However, with non−spherical conducting fillers, there may be a reduction in the percolation threshold of MWCNTs/PVDF to 0.0161 [25]. Notably, in the *n*Au−**f**MWCNTs/PVDF composite with an $f_{n\text{Au}-\text{fMWCTs}}$ of 0.008, an ε' value of 65.3 and a tanδ of approximately 0.216 were achieved, as shown in Fig. 11(b). This represents a substantial increase in dielectric response within the PVDF matrix composite, especially when compared with ceramic/polymer composites [10,13,14,16,17].

Fig. 12 illustrates the ac conductivity (σ_{ac}) of *n*Au−**f**MWCNTs/PVDF nanocomposites, in comparison to MWCNTs/PVDF nanocomposites. The σ_{ac} values at 1 kHz and 25 °C are summarized in Table 2. The σ_{ac} of MWCNTs/PVDF nanocomposites is significantly higher than that of *n*Au–**f**MWCNTs/PVDF nanocomposites by 2–4 orders of magnitude at the same filler volume fraction, corresponding to the notable changes observed in their tanδ values. As shown in Fig. 12 and Table 2, σ_{ac} increases with increasing filler volume fraction for all nanocomposite systems. This observation is similar to those reported in previous works [65–67]. The attachment of Au nanoparticles to the surface of **f**MWCNTs aids in filler dispersion within the polymer nanocomposites. This is attributed to the charge–induced repulsion, which increases the surface area of the composite, thereby reducing the tanδ. Additionally, the decrease in σ_{ac} is also a result of the Coulomb blockade effect. Surface modification of MWCNTs with Au nanoparticles has been effective in significantly reducing both tanδ and σ_{ac}. The increase in ε' should be associated with the number of free charges, which can induce interfacial polarization [1,24]. Furthermore, the increase in ε' can also be explained by the formation of micro–capacitors and percolation effect [43,44,63]. According to percolation theory, the properties transition from insulating to conducting [25,68,69]. This transition occurs when the concentration of the conductive phase becomes sufficiently high to form continuous pathways, leading to an immediate change in ε', tanδ, and σ_{ac} values [68,70].

Fig. 13 illustrates the ε', σ_{ac}, and tanδ values at 1 kHz for *n*Au−**f**MWCNTs/PVDF nanocomposites compared to MWCNTs/PVDF nanocomposites, as a function of filler volume fractions. For *n*Au−**f**MWCNTs/PVDF nanocomposites, these three parameters increase rapidly when the $f_{n\text{Au-fMWCNTs}}$ value exceeds 0.008. The electrical conductivity of *n*Au−**f**MWCNTs/PVDF nanocomposites, particularly near−percolation composite materials, has been studied due to the presence of conductive fillers. The conductivity is calculated using Equation (3):

$$\sigma = \sigma_0 (f - f_C)^q, \tag{3}$$

In this equation, σ and σ_0 represent the electrical conductivity of *n*Au−**f**MWCNTs/PVDF nanocomposites and constant value, f is the filler volume fraction, f_c is percolation threshold, and q is critical exponent. Our experimental data fits Equation (3), with $f_c = 0.008$ and $q = 1.272$, as shown in the inset of Fig. 13. The ε' value of MWCNTs/PVDF nanocomposites increases rapidly as the **f**MWCNTs value ranges from 0 to 0.005, indicating that the f_c for MWCNTs/PVDF nanocomposites is ≤ 0.005. Generally, the q value for a two−dimensional (2D) system is approximately 1.1–1.3, and for a three−dimensional (3D) system, it is between 1.6 and 2.0 [24]. This suggests that a 3D conductivity network in *n*Au−**f**MWCNTs/PVDF nanocomposites is formed through the contact between

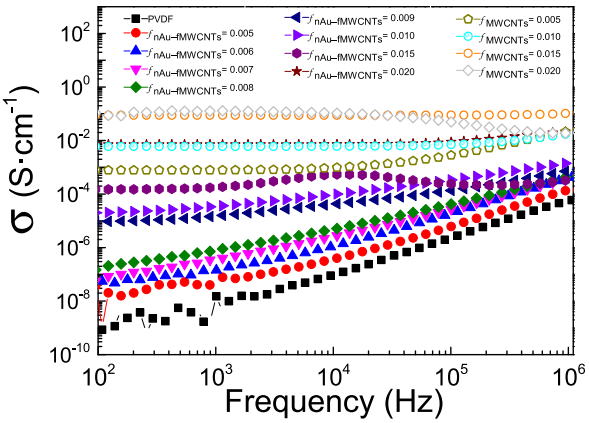

Fig. 12. Frequency dependence of σ_{ac} of *n*Au−**f**MWCNTs/PVDF polymer nanocomposites with various contents of *n*Au−**f**MWCNTs at ~25 °C compared to MWCNTs/PVDF nanocomposites.

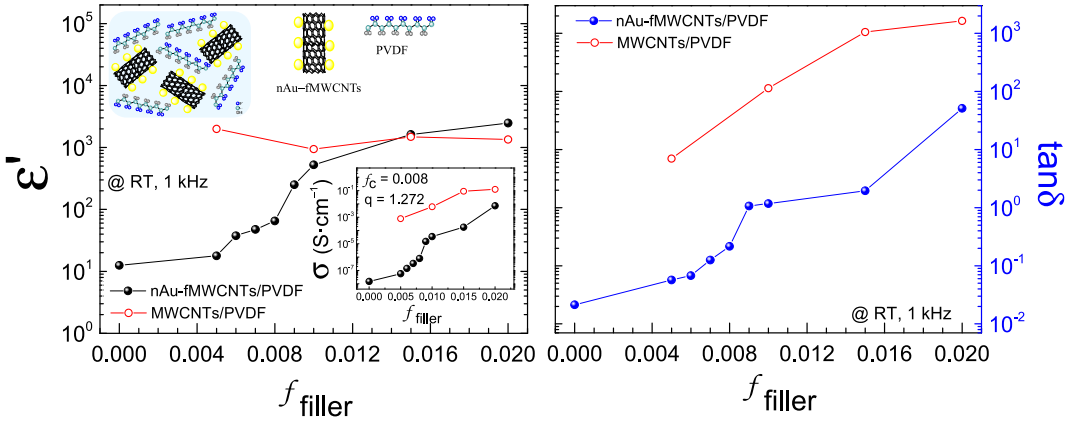

Fig. 13. (a) ε' and (b) tanδ at ~25 °C and 10^3 Hz for *n*Au−**f**MWCNTs/PVDF polymer nanocomposites with various contents of *n*Au−**f**MWCNTs compared to MWCNTs/PVDF nanocomposites; insert shows σ_{AC} as a function of $f_{nAu-fMWCNTs}$.

*n*Au−**f**MWCNTs. The low percolation threshold is likely due to the high aspect ratio of **f**MWCNTs, whose negative surface charges result in repulsion, assisting in uniform dispersion within the polymer matrix. This leads to a decrease in tanδ when the concentration of *n*Au−**f**MWCNTs/PVDF nanocomposites is less than 0.008, as shown in Fig. 13(b).

Fig. 14 presents the ε' and tanδ values for all the nanocomposite systems studied. The significantly increased tanδ values in the MWCNTs/PVDF polymer nanocomposites can be attributed to the accumulation of mobile charge carriers at the interface between the

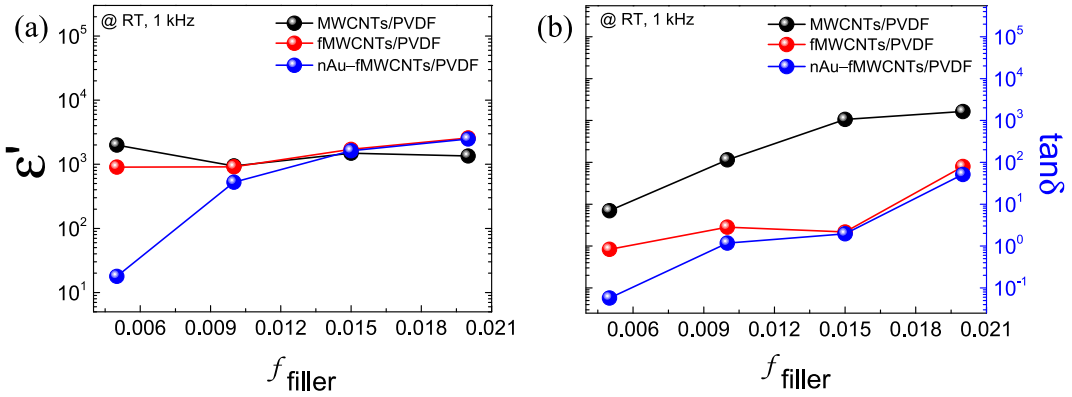

Fig. 14. Filler dependence of (a) ε' and (b) tanδ at ~25 °C and 10^3 Hz for all nanocomposite systems.

fillers and the PVDF polymer matrix, as well as the formation of a continuous conducting network. Conversely, the decreased tanδ values observed in the **f**MWCNTs/PVDF and *n*Au−**f**MWCNTs/PVDF nanocomposites can be attributed to improved dispersion resulting from surface modification through acid treatment. Notably, when the *n*Au−**f**MWCNTs loading is less than 0.009, a reduction in tanδ values is observed, as previously mentioned, especially when compared to the **f**MWCNTs and MWCNTs fillers at equivalent volume fractions. Factors contributing to lower tanδ values include charge distributions, dc conduction within the composites, dipole loss [43], quantum confinement effects, and Coulomb blockade [63]. These phenomena are likely a result of *n*Au particles being attached to the surface of **f**MWCNTs. The Coulomb blockade effect is notably observed in metallic nanoparticles with low-dimensional systems, particularly in Au nanoparticles. These nanoparticles exhibit electronic discontinuity with quantized values. Quantification of their electronic states reveals the emergence of novel features and phenomena. Studies have shown that the conductivity of Au nanoparticles diminishes as their size reduces to the nanometer scale. Specifically, Au nanoparticles with sizes ranging from 10 to 50 nm exhibited conductivities between 1.5 and 2.2×10^{-2} S/m [45]. As detailed in Table 2, the tanδ value of the *n*Au−**f**MWCNTs/PVDF nanocomposites was significantly lower compared to the **f**MWCNTs/PVDF composites at the same filler volume fraction. at equivalent filler volume fractions. Consequently, the insulating properties of Au nanoparticles can also impede the formation of conductive pathways, thereby reducing DC conduction and tanδ.

It is important to acknowledge that the dielectric properties of the *n*Au−**f**MWCNTs/PVDF nanocomposites were evaluated using a relatively low oscillation voltage of 0.5 V in our study. It is essential to recognize that in practical applications, these dielectric composites are typically subjected to much higher operating voltages. This disparity underscores the critical importance of high–voltage testing in the context of dielectric composite applications. Therefore, for future research endeavors, it is strongly advised to assess the electrical and dielectric properties of such materials under high field conditions. This approach aligns with methodologies employed in prior studies, as reported in previous works [71–73].

4. Conclusions

In summary, this study successfully synthesized PVDF nanocomposite films using *n*Au−**f**MWCNTs. The nanohybrids, produced through an adapted *Turkevich* method, demonstrated a favorable weight ratio and substantial improvements in dielectric properties. Detailed analyses confirmed the formation of *n*Au−**f**MWCNTs and their effective integration into the PVDF matrix at various filler concentrations. The novel three−phase percolative nanocomposites, formed by dispersing the *n*Au−**f**MWCNTs in DMF, showed enhanced interaction between the negatively charged *n*Au−**f**MWCNTs and the polar phases of PVDF. This interaction was further substantiated by zeta potential and FTIR analyses. A remarkable increase in ε' from 17.8 to 524.8 at 1 kHz was observed with filler loadings ranging from 0.005 to 0.01 vol%, highlighting the significant influence of the *n*Au−**f**MWCNTs. Moreover, despite the high ε', tanδ remained relatively low, increasing only marginally from 0.05 to 1.18. This balance between high ε' and low tanδ is attributed to the elevated permittivity of the *n*Au−**f**MWCNTs hybrid powder, the transition of PVDF to the β−phase, and the effects of interfacial polarization. Additionally, the restrained growth of *n*Au on the **f**MWCNTs and the prevention of conductive pathways within the polymer matrix were key factors in maintaining low tanδ values. The findings of this research provide significant insights into the development of high−performance dielectric materials. The enhanced properties of the PVDF nanocomposites, as demonstrated in this study, have potential applications in electronic and energy storage devices, where high permittivity and low dielectric loss are essential.

Data availability statement

Data will be made available on request.

CRediT authorship contribution statement

Kaniknun Sreejivungsa: Writing – original draft, Visualization, Methodology, Investigation, Formal analysis, Data curation, Conceptualization. **Prasit Thongbai:** Writing – review & editing, Writing – original draft, Visualization, Validation, Supervision, Resources, Project administration, Funding acquisition, Formal analysis, Conceptualization.

Declaration of competing interest

The authors declare that they have no known competing financial interests or personal relationships that could have appeared to influence the work reported in this paper.

Acknowledgments

This project was funded by the National Science, Research, and Innovation Fund (NSRF) and **the Fundamental** Fund **of Khon Kaen University**. This project was also supported by the Research and Graduate Studies Office of Khon Kaen University. K. Sreejivungsa would like to thank the Research Network NANOTEC (RNN) program of the National Nanotechnology Center (NANOTEC) and Khon Kaen University for her Ph.D. scholarship.

References

[1] Z.-M. Dang, J.-K. Yuan, J.-W. Zha, T. Zhou, S.-T. Li, G.-H. Hu, Fundamentals, processes and applications of high-permittivity polymer–matrix composites, Prog. Mater. Sci. 57 (2012) 660–723.
[2] P. Martins, A.C. Lopes, S. Lanceros-Mendez, Electroactive phases of poly(vinylidene fluoride): Determination, processing and applications, Prog. Polym. Sci. 39 (2014) 683–706.
[3] Prateek, V.K. Thakur, R.K. Gupta, Recent progress on ferroelectric polymer-based nanocomposites for high energy density capacitors: synthesis, dielectric properties, and future aspects, Chem. Rev. 116 (2016) 4260–4317.
[4] T. Zhou, J.W. Zha, R.Y. Cui, B.H. Fan, J.K. Yuan, Z.M. Dang, Improving dielectric properties of $BaTiO_3$/ferroelectric polymer composites by employing surface hydroxylated BaTiO(3) nanoparticles, ACS Appl. Mater. Interfaces 3 (2011) 2184–2188.
[5] A.C. Lopes, C.M. Costa, R.S.i. Serra, I.C. Neves, J.L.G. Ribelles, S. Lanceros-Méndez, Dielectric relaxation, ac conductivity and electric modulus in poly (vinylidene fluoride)/NaY zeolite composites, Solid State Ionics 235 (2013) 42–50.
[6] M.-m. Tao, F. Liu, B.-r. Ma, L.-x. Xue, Effect of solvent power on PVDF membrane polymorphism during phase inversion, Desalination 316 (2013) 137–145.
[7] D. Wang, Y. Bao, J.W. Zha, J. Zhao, Z.M. Dang, G.H. Hu, Improved dielectric properties of nanocomposites based on poly(vinylidene fluoride) and poly(vinyl alcohol)-functionalized graphene, ACS Appl. Mater. Interfaces 4 (2012) 6273–6279.
[8] X.-l. Xu, C.-j. Yang, J.-h. Yang, T. Huang, N. Zhang, Y. Wang, Z.-w. Zhou, Excellent dielectric properties of poly(vinylidene fluoride) composites based on partially reduced graphene oxide, Compos. B Eng. 109 (2017) 91–100.
[9] Q. Tan, P. Irwin, Y. Cao, Advanced dielectrics for capacitors, Ieej Transactions on Fundamentals and Materials 126 (2006) 1153–1159.
[10] Z.-M. Dang, H.-P. Xu, H.-Y. Wang, Significantly enhanced low-frequency dielectric permittivity in the $BaTiO_3$/poly(vinylidene fluoride) nanocomposite, Appl. Phys. Lett. 90 (2007) 012901.
[11] P. Kum−onsa, P. Thongbai, Dielectric properties of poly(vinylidene fluoride)-based nanocomposites containing a $LaFeO_3$ nanoparticle filler, J. Mater. Sci. Mater. Electron. 32 (2021) 13985–13993.
[12] S. Dash, R.N.P. Choudhary, M.N. Goswami, Enhanced dielectric and ferroelectric properties of PVDF-$BiFeO_3$ composites in 0–3 connectivity, J. Alloys Compd. 715 (2017) 29–36.
[13] C. Yang, H.-s. Song, D.-b. Liu, Effect of coupling agents on the dielectric properties of $CaCu_3Ti_4O_{12}$/PVDF composites, Compos. B Eng. 50 (2013) 180–186.
[14] S. Kaur, D.P. Singh, On the structural, dielectric and energy storage behaviour of PVDF-$CaCu_3Ti_4O_{12}$ nanocomposite films, Mater. Chem. Phys. 239 (2020) 122301.
[15] P. Kum−onsa, P. Thongbai, $Na_{1/3}Ca_{1/3}Bi_{1/3}Cu_3Ti_4O_{12}$/poly(vinylidene fluoride) composites with high dielectric permittivity and low dielectric loss, Mater. Chem. Phys. 256 (2020) 123664.
[16] P. Kum-onsa, P. Thongbai, Improved dielectric properties of poly(vinylidene fluoride) composites incorporating $Na_{1/2}Y_{1/2}Cu_3Ti_4O_{12}$ particles, Mater. Today Commun. 25 (2020) 101654.
[17] Y.-l. Su, C. Sun, W.-q. Zhang, H. Huang, Fabrication and dielectric properties of $Na_{0.5}Bi_{0.5}Cu_3Ti_4O_{12}$/poly(vinylidene fluoride) composites, J. Mater. Sci. 48 (2013) 8147–8152.
[18] Z.-M. Dang, H.-Y. Wang, B. Peng, C.-W. Nan, Effect of $BaTiO_3$ size on dielectric property of $BaTiO_3$/PVDF composites, J. Electroceram. 21 (2007) 381–384.
[19] B.-H. Fan, J.-W. Zha, D. Wang, J. Zhao, Z.-M. Dang, Size-dependent low-frequency dielectric properties in the $BaTiO_3$/poly(vinylidene fluoride) nanocomposite films, Appl. Phys. Lett. 100 (2012) 012903.
[20] K. Hayashida, Y. Matsuoka, Highly enhanced dielectric constants of barium titanate-filled polymer composites using polymer-grafted carbon nanotube matrix, Carbon 60 (2013) 506–513.
[21] Z.-M. Dang, J.-P. Wu, H.-P. Xu, S.-H. Yao, M.-J. Jiang, J. Bai, Dielectric properties of upright carbon fiber filled poly(vinylidene fluoride) composite with low percolation threshold and weak temperature dependence, Appl. Phys. Lett. 91 (2007) 072912.
[22] F. Dalmas, R. Dendievel, L. Chazeau, J.-Y. Cavaillé, C. Gauthier, Carbon nanotube-filled polymer composites. Numerical simulation of electrical conductivity in three-dimensional entangled fibrous networks, Acta Mater. 54 (2006) 2923–2931.
[23] C. Yang, Y. Lin, C.W. Nan, Modified carbon nanotube composites with high dielectric constant, low dielectric loss and large energy density, Carbon 47 (2009) 1096–1101.
[24] C.W. Nan, Y. Shen, J. Ma, Physical properties of composites near percolation, Annu. Rev. Mater. Res. 40 (2010) 131–151.
[25] L. Wang, Z.-M. Dang, Carbon nanotube composites with high dielectric constant at low percolation threshold, Appl. Phys. Lett. 87 (2005) 042903.
[26] T. Zhou, J.-W. Zha, Y. Hou, D. Wang, J. Zhao, Z.-M. Dang, Surface-functionalized MWNTs with Emeraldine base: preparation and improving dielectric properties of polymer nanocomposites, ACS Appl. Mater. Interfaces 3 (2011) 4557–4560.
[27] S. Song, S. Xia, S. Jiang, X. Lv, S. Sun, Q. Li, A facile strategy to enhance the dielectric and mechanical properties of MWCNTs/PVDF composites with the aid of MMA-co-GMA copolymer, Materials (2018) 11.
[28] Y. Zhen, J. Arredondo, G.-L. Zhao, Unusual dielectric loss properties of carbon nanotube—Polyvinylidene fluoride composites in low frequency Region (100 Hz $< f <$ 1 MHz), Open J. Org. Polym. Mater. 3 (2013) 99–103.
[29] G.-W. Lee, J. Kim, J. Yoon, J.-S. Bae, B.C. Shin, I.S. Kim, W. Oh, M. Ree, Structural characterization of carboxylated multi-walled carbon nanotubes, Thin Solid Films 516 (2008) 5781–5784.
[30] A. Amiri, M. Shanbedi, H. Eshghi, S.Z. Heris, M. Baniadam, Highly dispersed multiwalled carbon nanotubes decorated with Ag nanoparticles in water and experimental investigation of the Thermophysical properties, J. Phys. Chem. C 116 (2012) 3369–3375.
[31] J. Lee, M. Kim, C.K. Hong, S.E. Shim, Measurement of the dispersion stability of pristine and surface-modified multiwalled carbon nanotubes in various nonpolar and polar solvents, Meas. Sci. Technol. 18 (2007) 3707–3712.
[32] J. Yu, N. Grossiord, C.E. Koning, J. Loos, Controlling the dispersion of multi-wall carbon nanotubes in aqueous surfactant solution, Carbon 45 (2007) 618–623.
[33] S. Gómez, N.M. Rendtorff, E.F. Aglietti, Y. Sakka, G. Suárez, Surface modification of multiwall carbon nanotubes by sulfonitric treatment, Appl. Surf. Sci. 379 (2016) 264–269.
[34] D.S. Ahmed, A.J. Haider, M.R. Mohammad, Comparesion of functionalization of multi-walled carbon nanotubes treated by Oil Olive and nitric acid and their characterization, Energy Proc. 36 (2013) 1111–1118.
[35] V. Datsyuk, M. Kalyva, K. Papagelis, J. Parthenios, D. Tasis, A. Siokou, I. Kallitsis, C. Galiotis, Chemical oxidation of multiwalled carbon nanotubes, Carbon 46 (2008) 833–840.
[36] V.N. Khabashesku, Covalent functionalization of carbon nanotubes: synthesis, properties and applications of fluorinated derivatives, Russ. Chem. Rev. 80 (2011) 705–725.
[37] Y.-T. Shieh, J.-Y. Chen, Y.-K. Twu, W.-J. Chen, The effect of pH and ionic strength on the dispersion of carbon nanotubes in poly(acrylic acid) solutions, Polym. Int. 61 (2012) 554–559.
[38] F. Ahmadpoor, S.M. Zebarjad, K. Janghorban, Decoration of multi-walled carbon nanotubes with silver nanoparticles and investigation on its colloid stability, Mater. Chem. Phys. 139 (2013) 113–117.
[39] B. Xue, P. Chen, Q. Hong, J. Lin, K.L. Tan, Growth of Pd, Pt, Ag and Au nanoparticles on carbon nanotubes, J. Mater. Chem. 11 (2001) 2378–2381.
[40] F.W.A. Zulikifli, H. Yazid, M.Z.B.A. Halim, A.M.M. Jani, Synthesis of gold nanoparticles on multi-walled carbon nanotubes (Au-MWCNTs) via deposition precipitation method, AIP Conf. Proc. 1877 (2017) 070003.
[41] R. Zhang, M. Hummelgård, H. Olin, Simple and efficient gold nanoparticles deposition on carbon nanotubes with controllable particle sizes, Mater. Sci. Eng. B 158 (2009) 48–52.
[42] V. Duc Chinh, G. Speranza, C. Migliaresi, N. Van Chuc, V. Minh Tan, N.-T. Phuong, Synthesis of gold nanoparticles decorated with multiwalled carbon nanotubes (Au-MWCNTs) via Cysteaminium chloride functionalization, Sci. Rep. 9 (2019) 5667.

[43] R. Kumaran, S.D. kumar, N. Balasubramanian, M. Alagar, V. Subramanian, K. Dinakaran, Enhanced electromagnetic Interference shielding in a Au–MWCNT composite nanostructure dispersed PVDF Thin films, J. Phys. Chem. C 120 (2016) 13771–13778.
[44] K. Rengaswamy, V.K. Asapu, A. Muthukaruppan, D.K. Sakthivel, S. Venkatachalam, D. Kannaiyan, Enhanced shielding of electromagnetic radiations with flexible, light-weight, and conductive Ag-Cu/MWCNT/rGO architected PVDF nanocomposite films, Polym. Adv. Technol. 32 (2021) 3759–3769.
[45] M.A.K. Abdelhalim, M.M. Mady, M.M. Ghannam, Rheological and dielectric properties of different gold nanoparticle sizes, Lipids Health Dis. 10 (2011) 208.
[46] Z.M. Dang, L. Wang, Y. Yin, Q. Zhang, Q.Q. Lei, Giant dielectric permittivities in functionalized carbon-nanotube/electroactive-polymer nanocomposites, Adv. Mater. 19 (2007) 852–857.
[47] F. Avilés, J.V. Cauich-Rodríguez, L. Moo-Tah, A. May-Pat, R. Vargas-Coronado, Evaluation of mild acid oxidation treatments for MWCNT functionalization, Carbon 47 (2009) 2970–2975.
[48] J. Turkevich, P.C. Stevenson, J. Hillier, A study of the nucleation and growth processes in the synthesis of colloidal gold, Discuss. Faraday Soc. 11 (1951) 55–75.
[49] K.N. Chaudhari, S. Chaudhari, J.-S. Yu, Synthesis and supercapacitor performance of Au-nanoparticle decorated MWCNT, J. Electroanal. Chem. 761 (2016) 98–105.
[50] C. Ribeiro, C.M. Costa, D.M. Correia, J. Nunes-Pereira, J. Oliveira, P. Martins, R. Gonçalves, V.F. Cardoso, S. Lanceros-Méndez, Electroactive poly(vinylidene fluoride)-based structures for advanced applications, Nat. Protoc. 13 (2018) 681–704.
[51] M.M.J. Kimling, B. Okenve, V. Kotaidis, H. Ballot, A. Plech, Turkevich method for gold nanoparticle synthesis revisited, Phys. Chem. B 110 (2006) 15700–15707.
[52] X. Liu, M. Atwater, J. Wang, Q. Huo, Extinction coefficient of gold nanoparticles with different sizes and different capping ligands, Colloids Surf. B Biointerfaces 58 (2007) 3–7.
[53] X.S. Xiaohui Ji, Jun Li, Yubai Bai, Wensheng Yang, Xiaogang Peng, Size control of gold nanocrystals in citrate reduction:the third role of citrate, Am. Chem. Soc. 129 (2007) 13939–13948.
[54] J. Piella, N.G. Bastús, V. Puntes, Size-controlled synthesis of sub-10-nanometer citrate-stabilized gold nanoparticles and related optical properties, Chem. Mater. 28 (2016) 1066–1075.
[55] H. Tyagi, A. Kushwaha, A. Kumar, M. Aslam, A facile pH controlled citrate-based reduction method for gold nanoparticle synthesis at room temperature, Nanoscale Res. Lett. 11 (2016) 362.
[56] J. Jiang, G. Oberdörster, P. Biswas, Characterization of size, surface charge, and agglomeration state of nanoparticle dispersions for toxicological studies, J. Nanoparticle Res. 11 (2009) 77–89.
[57] K. Sreejivungsa, N. Phromviyo, E. Swatsitang, P. Thongbai, Characterizations and significantly enhanced dielectric properties of PVDF polymer nanocomposites by incorporating gold nanoparticles deposited on $BaTiO_3$ nanoparticles, Polymers 13 (2021).
[58] X. Ji, X. Song, J. Li, Y. Bai, W. Yang, X. Peng, Size control of gold nanocrystals in citrate reduction: the third role of citrate, J. Am. Chem. Soc. 129 (2007) 13939–13948.
[59] M. Tran, R. DePenning, M. Turner, S. Padalkar, Effect of citrate ratio and temperature on gold nanoparticle size and morphology, Mater. Res. Express 3 (2016) 105027.
[60] N.T. Abdel-Ghani, G.A. El-Chaghaby, F.S. Helal, Individual and competitive adsorption of phenol and nickel onto multiwalled carbon nanotubes, J. Adv. Res. 6 (2015) 405–415.
[61] X. Cai, T. Lei, D. Sun, L. Lin, A critical analysis of the α, β and γ phases in poly(vinylidene fluoride) using FTIR, RSC Adv. 7 (2017) 15382–15389.
[62] V. R P, D.V. Khakhar, A. Misra, Studies on α to β phase transformations in mechanically deformed PVDF films, J. Appl. Polym. Sci. 117 (2010) 3491–3497.
[63] L. Xie, X. Huang, B.-W. Li, C. Zhi, T. Tanaka, P. Jiang, Core–satellite Ag@$BaTiO_3$ nanoassemblies for fabrication of polymer nanocomposites with high discharged energy density, high breakdown strength and low dielectric loss, Phys. Chem. Chem. Phys. 15 (2013) 17560–17569.
[64] J. Lin, P. Zhang, W. Yang, Z. Xie, Y. Liu, H. Lin, X. Li, Q. Lei, Novel potassium sodium niobate/polyimide functional composite films with high dielectric permittivity, Polym. Compos. 35 (2014) 969–974.
[65] Y. Wang, J. Chen, Y. Shen, T. Wang, Y. Ni, Z. Zhang, L. Sun, B. Ji, B. Wang, Control of conductive and mechanical performances of poly(amide-imide) composite films utilizing synergistic effect of polyaniline and multi-walled carbon nanotube, Polym. Eng. Sci. 59 (2019) E224–E230.
[66] Z. Fan, Y. Wang, J. Jeon, S.D. Kim, Y. Fang, X. Shi, Z. Luo, H. Ohkita, B. Wang, Enhancing multiwalled carbon nanotubes/poly(amide-imide) interfacial strength through grafting polar conjugated polymer on multiwalled carbon nanotubes, Surface. Interfac. 32 (2022) 102130.
[67] Y. Fang, H. Yu, Y. Wang, Z. Zhang, C. Zhuang, G. Fang, Z. Luo, B. Zhang, B. Wang, Simultaneous improvement of mechanical and conductive properties of poly (amide-imide) composites using carbon nano-materials with different morphologies, J. Polym. Eng. 40 (2020) 806–814.
[68] Z.-M. Dang, Y.-H. Lin, C.-W. Nan, Novel ferroelectric polymer composites with high dielectric constants, Adv. Mater. 15 (2003) 1625–1629.
[69] Z.-M.D. Hong-Tao Song, Enhanced electrical properties in percolative low-density polyethylene/carbon nanotubes nanocomposites, IEEE Trans. Dielectr. Electr. Insul. 17 (2010) 645–652.
[70] X. Huang, P. Jiang, L. Xie, Ferroelectric polymer/silver nanocomposites with high dielectric constant and high thermal conductivity, Appl. Phys. Lett. 95 (2009) 242901.
[71] W. Zhou, G. Cao, M. Yuan, S. Zhong, Y. Wang, X. Liu, D. Cao, W. Peng, J. Liu, G. Wang, Z.-M. Dang, B. Li, Core–shell engineering of conductive fillers toward enhanced dielectric properties: a universal polarization mechanism in polymer conductor composites, Adv. Mater. 35 (2023) 2207829.
[72] T. Yao, W. Zhou, G. Cao, W. Peng, J. Liu, X. Dong, X. Chen, Y. Zhang, Y. Chen, M. Yuan, Engineering of core@double-shell structured Zn@ZnO@PS particles in poly(vinylidene fluoride) composites towards significantly enhanced dielectric performances, J. Appl. Polym. Sci. 140 (2023) e53772.
[73] V. Bakola, O. Kotrotsiou, A. Ntziouni, D. Dragatogiannis, N. Plakantonaki, C. Trapalis, C. Charitidis, C. Kiparissides, Development of composite nanostructured electrodes for water desalination via membrane capacitive deionization, Macromol. Rapid Commun. (2024) 2300640 n/a.